

Structural and Superconducting Properties in the Te-doped Spinel

CuRh_2Se_4

Kuan Li^a, Lingyong Zeng^a, Longfu Li^a, Rui Chen^a, Peifeng Yu^a, Kangwang Wang^a,

Chao Zhang^a, Zaichen Xiang^a, Huixia Luo^{a,b,c,d}*

^aSchool of Materials Science and Engineering, Sun Yat-sen University, No. 135,
Xingang Xi Road, Guangzhou, 510275, P. R. China

^bState Key Laboratory of Optoelectronic Materials and Technologies, Sun Yat-sen
University, No. 135, Xingang Xi Road, Guangzhou, 510275, P. R. China

^cKey Lab of Polymer Composite & Functional Materials, Sun Yat-sen University, No.
135, Xingang Xi Road, Guangzhou, 510275, P. R. China

^dGuangdong Provincial Key Laboratory of Magnetoelectric Physics and Devices, Sun
Yat-sen University, No. 135, Xingang Xi Road, Guangzhou, 510275, P. R. China

ABSTRACT In this paper, we discuss the impact of tellurium (Te) doping on the spinel superconductor CuRh_2Se_4 . We conducted a comprehensive evaluation of the structural and superconducting properties of the system using various techniques, including X-ray diffraction (XRD), resistivity, magnetization, and specific heat measurements. Based on our XRD analysis, we found that the spinel superconductor $\text{CuRh}_2\text{Se}_{4-x}\text{Te}_x$ ($0 \leq x \leq 0.28$) crystallizes in the space group $Fd\bar{3}m$ (227), while the layered compound $\text{CuRh}_2\text{Se}_{4-x}\text{Te}_x$ ($2.8 \leq x \leq 4.0$) crystallizes in the space group $P\bar{3}m1$ (164). The upper critical magnetic field can be increased from 0.95(2) T for CuRh_2Se_4 to 3.44(1) T for $\text{CuRh}_2\text{Se}_{3.72}\text{Te}_{0.28}$ by doping with elemental Te. However, the layered compound $\text{CuRh}_2\text{Se}_{4-x}\text{Te}_x$ ($2.8 \leq x \leq 4.0$) did not exhibit superconducting properties. Besides, the specific heat measurements of $\text{CuRh}_2\text{Se}_{4-x}\text{Te}_x$ ($x = 0, 0.1, 0.28$) indicate that the Te element doping affects the electronic structure and interactions of the material and breaks the stability of the superconducting pairing, which leads to a decrease in the T_c . Finally, we show the electronic phase diagram of T_c with Te doping to summarise our findings.

KEYWORDS: Superconductivity; Spinel; Transition metal telluride; Electronic phase diagram

INTRODUCTION

Spinel is a type of material that has great potential for various applications. It has excellent electrical, magnetic, and thermal properties, making it relevant in many fields. Spinel exhibits unique physical properties, including multiferroicity, magnetostriction, and Kerr rotation [1-6], which have attracted much attention from researchers. The spinel structure is described by AB_2X_4 , where metal ions occupy the A and B positions, and the X position is occupied by oxygen, sulfur, selenium, or tellurium. Spinel compounds have the potential for various technological applications due to their fascinating physical characteristics. Despite discovering several thousand spinels, only a tiny fraction of them have demonstrated superconductivity.

Spinel is a crucial superconductor material that holds great potential for applications in various fields [7-29]. The cubic spinel compounds $CuRh_2Se_4$ and $CuRh_2S_4$ were reported to exhibit superconductivity in 1967 by van Maaren et al. [7] and Robbins et al. [8], with superconducting transition temperature (T_c) of 3.4 K and 4.7 K, respectively. After a few years, the bulk superconducting oxide spinel $LiTi_2O_4$ was discovered and had a T_c of 13.7 K, which set a record for the highest T_c among the spinel compound family [9]. Recently, superconductivity has also been observed in $MgTi_2O_4$ oxide spinel films grown on $MgAl_2O_4$ substrates, achieved through superlattice engineering of $MgTi_2O_4$ and $SrTiO_3$ [10]. Other spinel superconductors that have been reported, including electron-doped $CuIr_2S_4$ and $CuIr_2Se_4$, as well as the undoped ternary sulpospinel superconductors, $CuCo_2S_4$ [11-19, 27, 28]. The CuV_2S_4

compound, which has a cubic spinel structure composed of copper and sulfur, exhibits three distinct charge density wave (CDW) states at different temperatures: T_{CDW1} at 50 K, T_{CDW2} at 75 K, and T_{CDW3} at 90 K. These different states suggest that the phase transition in this compound may be caused by the behavior of electrons within its structure. And the T_c of CuV_2S_4 is 3.20 - 4.45 K [21, 22]. Recently, our group found that Pt doping can significantly enhance the upper critical magnetic field, in which the upper critical magnetic field $\mu_0 H_{c2}(0)$ increased from 0.6 T for the undoped CuRh_2Se_4 sample to 4.93 T for the Pt-doped composition $\text{Cu}(\text{Rh}_{0.94}\text{Pt}_{0.06})\text{Se}_4$ [29].

On the other hand, the introduction of Tellurium (Te) significantly influences both the crystal structure and the properties of the superconducting materials. For example, Te doping significantly impacts the critical temperature T_c , critical current density J_c , and flux pinning energy U of FeSe single crystals. Suitable Te doping can increase the J_c and U . Nevertheless, excessive Te doping leads to an increase in non-superconducting areas, which results in a swift reduction in both flux pinning energy and critical current density [30]. The T_c of $\text{Fe}_y\text{Se}_{1-x}\text{Te}_x$ films is intricately linked to the chemical composition, with Fe vacancies playing a crucial role in promoting higher T_c values [31]. The magnetic field dependence of the resistive transition in polycrystalline $\alpha\text{-FeSe}_{1-x}$ and $\text{FeSe}_{1-x}\text{Te}_x$ suggests that Te doping causes the system to become more two-dimensional and significantly enhances the upper critical field value, whereas the FeSe system behaves more like a 3D superconductor where Te replaces Se enlarging the lattice, increasing the T_c , and also greatly increasing the $\mu_0 H_{c2}(0)$. This great enhancement may stem from the more 2D-like properties in the tellurium-doped system.

When α -FeSe is doped with 70 % Te, $\mu_0 H_{c2}(0)$ is enhanced to 96.9 Tesla, well beyond the Pauli paramagnetic limit, estimated to be $\mu_0 H^{\text{Pauli}} = 4kT/\pi\mu_0 = 28.79$ Tesla, providing more insight into the unconventional pairing mechanism that plays a role in superconductors [32]. In the previous study, Te-doped 2H-NbSe₂ can cause a new type of superconducting material, 1T-NbTeSe [33], or new compositions 2H-NbSe_{2-x}Te_x [34]. These findings suggest that Te doping can significantly change the structural or physical properties.

Motivated by the research above, we propose to use Te doping spinel CuRh₂Se₄ and thus, design a series of CuRh₂Se_{4-x}Te_x. In this paper, we investigated the structure and physical properties of CuRh₂Se_{4-x}Te_x by X-ray diffraction, resistivity, magnetic susceptibility, and specific heat measurements.

EXPERIMENT

Polycrystalline CuRh₂Se_{4-x}Te_x samples were fabricated through a conventional solid-state reaction method. Stoichiometric ratios of Cu (99.9%), Rh (99.95%), Se (>99.9%), and Te (99.999%) were combined in quartz tubes. Subsequently, the quartz tubes underwent a ten-day heating process at 850 °C within a high vacuum setting (< 1 × 10⁻¹ MPa). The resulting powder samples were meticulously reprocessed, pelletized, and sintered at 850 °C for 48 hours.

The crystal structure was confirmed using XRD analysis. Data was collected from 10° to 100° with a step width of 0.01 ° and a constant scan speed of 1 °/min at room

temperature, utilizing the MiniFlex instrument from Rigaku with Cu K α radiation. The XRD patterns were refined via the Rietveld method using the FULLPROF suite package software. To characterize the morphology and microstructure, scanning electron microscopy (SEM) and energy-dispersive X-ray spectroscopy (EDS) analysis were conducted using the EVO system from Zeiss. For further analysis, resistivity measurements, zero-field-cooling (ZFC) magnetic susceptibility studies, and specific heat evaluations were carried out using the Quantum Design physical property measurement system DynaCool. Heat capacity measurements in the range of 1.8 K - 6 K and electrical resistivity assessments on rectangular samples ($4.5 \times 1.3 \times 0.6$ mm) were performed using the four-probe method on the Quantum Design physical property measuring system (PPMS). Additionally, magnetic susceptibilities were measured using the PPMS. The T_c was determined from the specific heat capacity $C_p(T)$ through the equal entropy construction.

RESULTS AND ANALYSIS

The series of polycrystalline XRD spectra and correlation analysis of $\text{CuRh}_2\text{Se}_{4-x}\text{Te}_x$ are shown in **Fig. 1**. XRD analysis at room temperature indicates that all $\text{CuRh}_2\text{Se}_{4-x}\text{Te}_x$ ($0 \leq x \leq 0.28$) samples are cubic phase, and the space group is $Fd\bar{3}m$ (227). Room temperature XRD Rietveld refinement of all samples revealed a strong correlation with the spinel CuRh_2Se_4 crystal structure (PDF card number: 04-0058682), although minor RhSe_2 impurities were detected in some samples. On the other hand, XRD results show that the powder diffraction pattern of the $\text{CuRh}_2\text{Se}_{4-x}\text{Te}_x$ ($0 \leq x \leq 0.28$) sample is mainly

spinel phase with space group $Fd\bar{3}m$ (227). The trigonal phase begins to appear in the $0.28 < x < 2.8$ region, indicating that the spinel phase and the layered trigonal phase coexist. The main layered trigonal phase with space group $P\bar{3}m1$ (164) is obtained in the doped region of $2.8 \leq x \leq 4.0$. The peaks around 35° were zoomed as depicted on the right side of **Fig. 1(a)**. When the doping amount of Te increases gradually, the obvious peaks shift to the left. According to Bragg's law $2d\sin\theta = n\lambda$, it is not difficult to explain that because the ionic radius of Te is larger than that of Se, the crystal plane spacing gradually increases with the increase of Te doping amount. **Fig. 1(b)** illustrates the lattice parameters exhibiting a remarkable linear correlation with Te doping content. **Fig. 1(c)**, the XRD Rietveld refinement of the sample $\text{CuRh}_2\text{Se}_{3.85}\text{Te}_{0.15}$ at room temperature is presented. Subsequently, employing Thompson-Cox-Hastings pseudo-Voigt peak shapes, we conduct a quantitative analysis of the XRD data using the FULLPROF software to determine the lattice parameters. The lattice parameter increased from $10.2645(4) \text{ \AA}$ for CuRh_2Se_4 to $10.3092(5) \text{ \AA}$ for $\text{CuRh}_2\text{Se}_{3.72}\text{Te}_{0.28}$. Further refined data for other compositions in the system can be found in **Fig. S2**. **Fig. 1(c)** internal shows the crystal structure of $\text{CuRh}_2\text{Se}_{4-x}\text{Te}_x$ ($0 \leq x \leq 0.28$), where the Te element partially replaces the Se element. Furthermore, the atomic ratios obtained from EDXS confirmed that the synthesized compounds were very close to the target compositions, as shown in **Table S1**. Additionally, EDXS mapping, as shown in **Fig. S1**, indicated that the polycrystalline samples exhibited uniformity. The XRD pattern of the highly doped level ($2.8 \leq x \leq 4.0$) of the layered compound $\text{CuRh}_2\text{Se}_{4-x}\text{Te}_x$ is shown in **Fig. 2 (a)**. It can be observed that the peak around 31° is amplified. As the

doping level of Te gradually increases, a noticeable shift of the peak to the left can be observed. Similarly, according to Bragg's law $2d\sin\theta = n\lambda$, it can be easily explained that as the doping level of Te increases, the interplanar spacing gradually increases due to the smaller ionic radius of Se compared to Te. All $\text{CuRh}_2\text{Se}_{4-x}\text{Te}_x$ ($2.8 \leq x \leq 4.0$) samples crystallized in the space group $P\bar{3}m1$ (164). The relationship between the lattice parameter and Te doping content is well represented by a linear function, as depicted in **Fig. 2(b)**. At room temperature, a representative sample of $\text{CuRh}_2\text{Se}_{1.2}\text{Te}_{2.8}$ was analyzed via XRD Rietveld refinement, as **Fig. 2(c)** displays the results. Then, the XRD data were quantitatively analyzed using FULLPROF software to determine the lattice parameters. The lattice parameter increased from 3.8307(3) Å for $\text{CuRh}_2\text{Se}_{1.2}\text{Te}_{2.8}$ to 4.0116(2) Å for CuRh_2Te_4 . In **Fig. 2(c)**, the internal view depicts the crystal structure of $\text{CuRh}_2\text{Se}_{4-x}\text{Te}_x$, where the value of x ranges from 2.8 to 4.0. Additionally, Cu ions are inserted between layers.

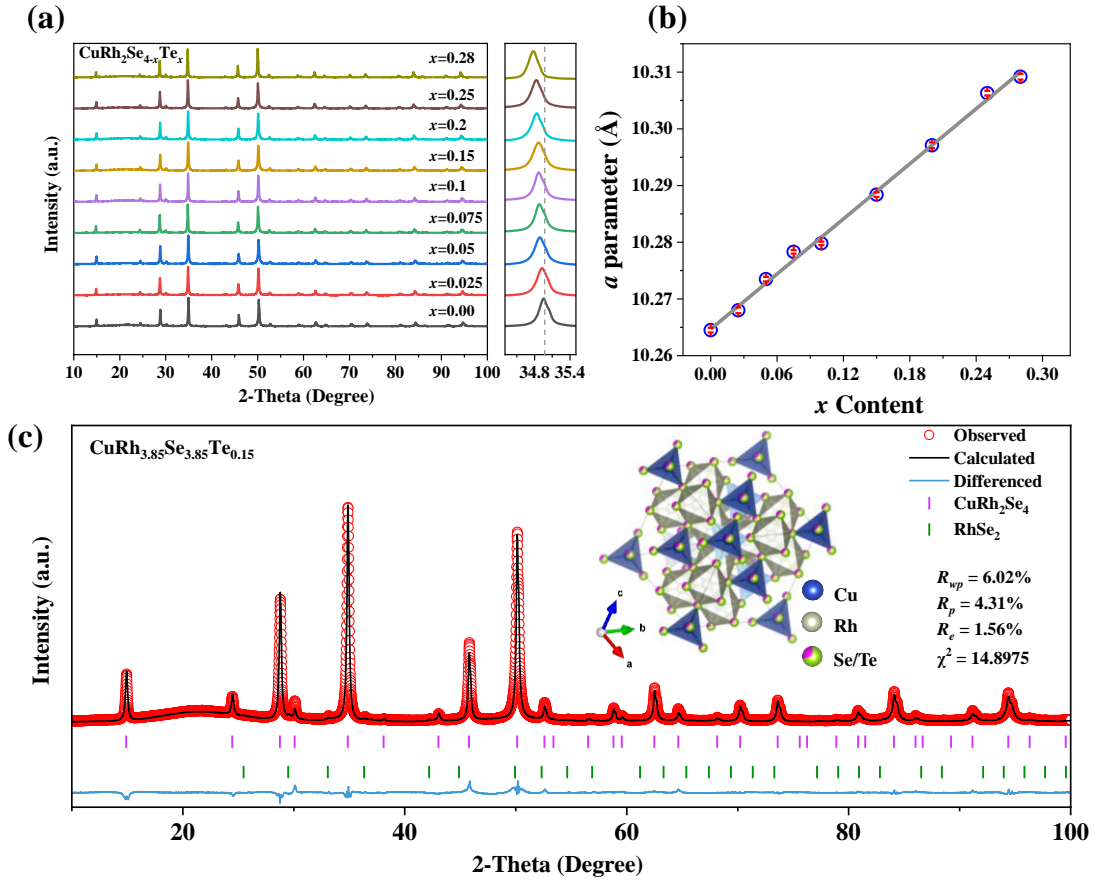


Fig. 1. Structural characterization and analysis of the spinel $\text{CuRh}_2\text{Se}_{4-x}\text{Te}_x$ ($0 \leq x \leq 0.28$). (a) Powder X-ray diffraction patterns for the spinel $\text{CuRh}_2\text{Se}_{4-x}\text{Te}_x$ ($0 \leq x \leq 0.28$). (b) Variation of the calculated lattice parameters a with Te-doping (c) Rietveld refinement profile of the XRD of the spinel $\text{CuRh}_2\text{Se}_{3.85}\text{Te}_{0.15}$, the crystal structure for the spinel $\text{CuRh}_2\text{Se}_{4-x}\text{Te}_x$ ($0 \leq x \leq 0.28$) samples with space group $Fd\bar{3}m$ is shown in Fig. 1c.

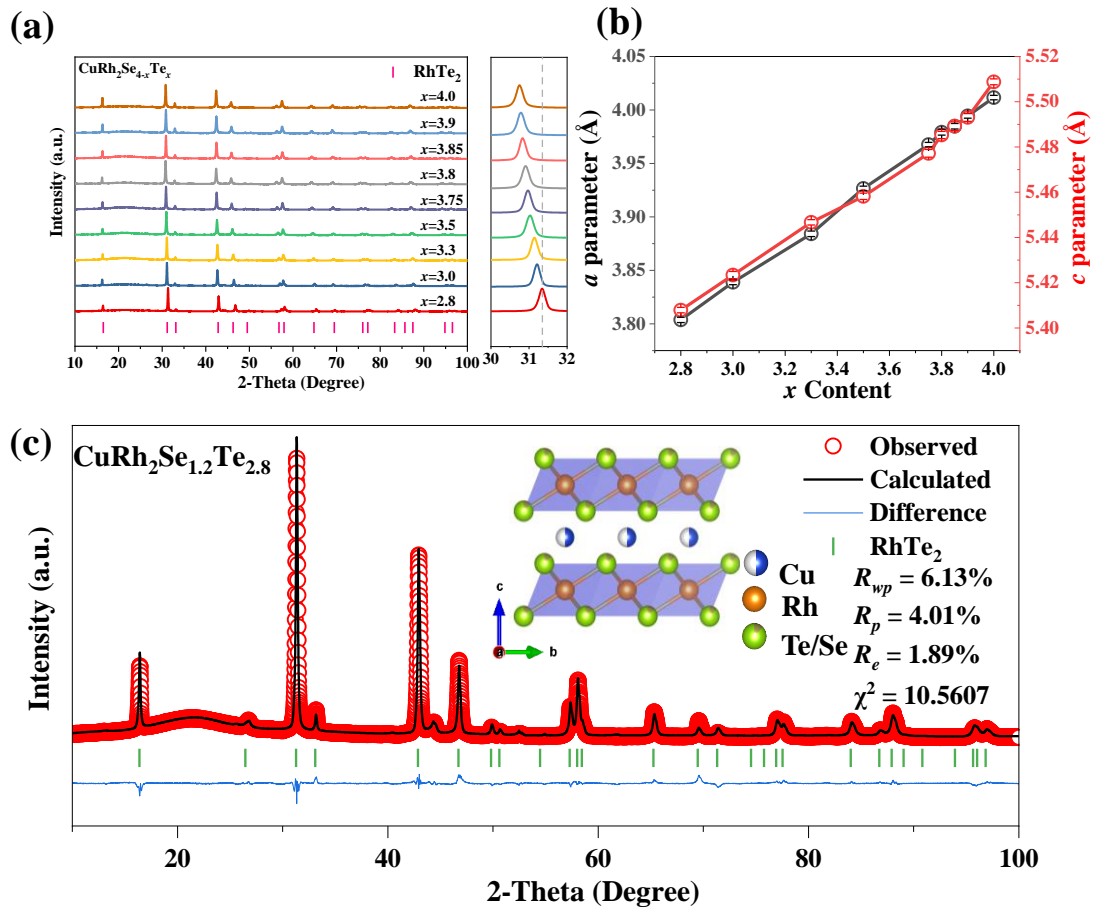


Fig. 2. Structural characterization and analysis of the layer compound $\text{CuRh}_2\text{Se}_{4-x}\text{Te}_x$ ($2.8 \leq x \leq 4.0$). (a) Powder XRD patterns for the layer compound $\text{CuRh}_2\text{Se}_{4-x}\text{Te}_x$ ($2.8 \leq x \leq 4.0$). (b) Variation of the calculated lattice parameters a and c with Te-doping. (c) Rietveld refinement profile of the XRD of the layer compound $\text{CuRh}_2\text{Se}_{1.2}\text{Te}_{2.8}$, the crystal structure for the layer compound $\text{CuRh}_2\text{Se}_{4-x}\text{Te}_x$ ($2.8 \leq x \leq 4.0$) samples with space group $P\bar{3}m1$ is shown in Fig. 2c.

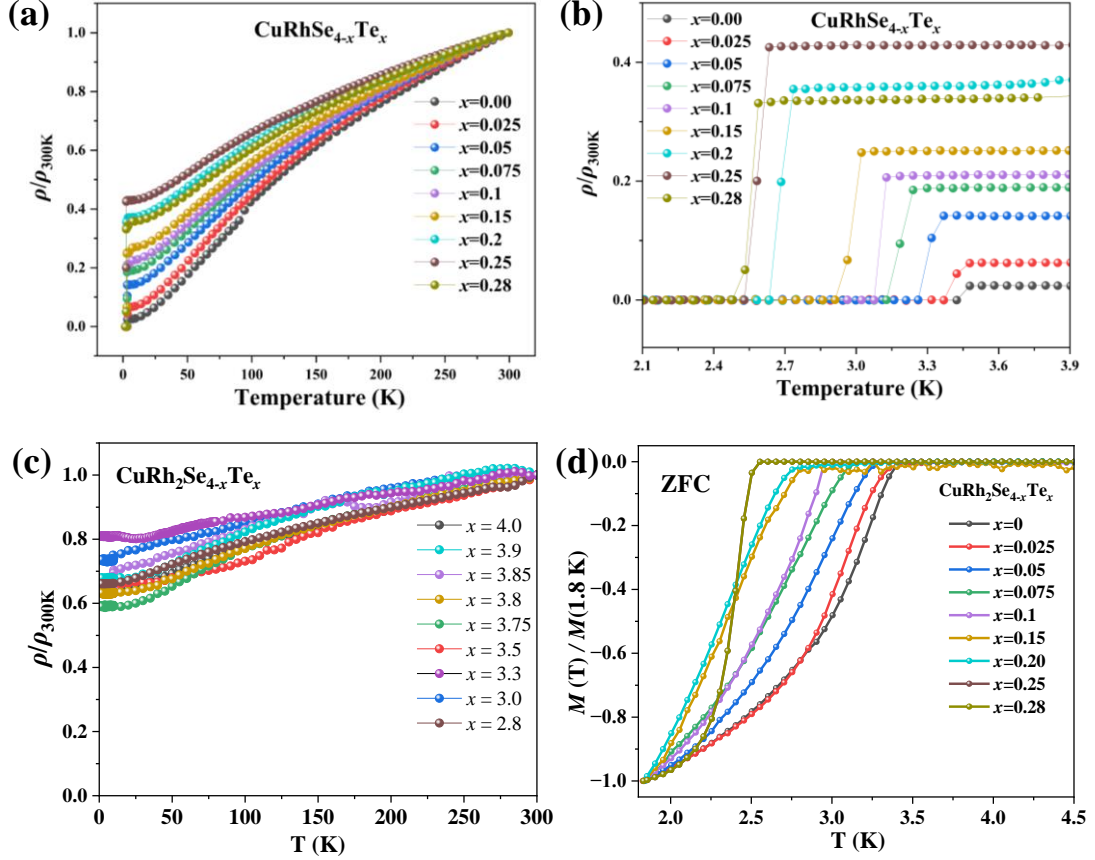


Fig. 3. (a) Temperature dependence of normalized ρ/ρ_{300K} of $\text{CuRh}_2\text{Se}_{4-x}\text{Te}_x$ ($0 \leq x \leq 0.28$). (b) Temperature dependence of normalized ρ/ρ_{300K} of $\text{CuRh}_2\text{Se}_{4-x}\text{Te}_x$ ($0 \leq x \leq 0.28$) at 2.1 – 3.9 K. (c) Temperature dependence of normalized ρ/ρ_{300K} of $\text{CuRh}_2\text{Se}_{4-x}\text{Te}_x$ ($2.8 \leq x \leq 4.0$). (d) Magnetic susceptibilities for the spinel $\text{CuRh}_2\text{Se}_{4-x}\text{Te}_x$ ($0 \leq x \leq 0.28$) samples at the superconducting transitions under a 30 Oe magnetic field.

The resistivity of $\text{CuRh}_2\text{Se}_{4-x}\text{Te}_x$ polycrystalline samples was measured at temperatures ranging from 300 K to 1.8 K. For the $\text{CuRh}_2\text{Se}_{4-x}\text{Te}_x$ sample, the highest T_c of 3.5 K was observed in the parent CuRh_2Se_4 , which is also consistent with that reported in the previous literature [13, 29]. However, superconductivity is inhibited

after Te doping and regularly decreases with increasing Te content. **Fig. 3(a)** provides a detailed illustration of the superconducting transition across a wide temperature range from 1.8 K to 300 K, whereas **Fig. 3(b)** depicts the resistivity trend at lower temperatures spanning from 2.1 to 3.9 K. The T_c was defined as a resistivity of 50 %. When $x = 0$, T_c reaches a maximum of 3.5 K; when $x = 0.15$, T_c gradually decreases to about 3 K with the increase of Te content, and when x reaches the maximum doping level of 0.28, T_c finally drops to about 2.5 K. **Fig. S3** shows the phase plot of the change in superconducting transition temperature T_c with the amount of Te doping. RRR is generally defined as the ratio of resistance measured at 273 K (freezing point of water) and 4.2 K (boiling point of helium at standard atmospheric pressure) [35]. Here, we define the residual resistivity ratio at 300 K and 5 K ($RRR = R_{300K}/R_{5K}$). **Table S2** summarizes the T_c and RRR values of $\text{CuRh}_2\text{Se}_{4-x}\text{Te}_x$ ($0 \leq x \leq 0.28$) samples. **Fig. S4** displays the RRR of each $\text{CuRh}_2\text{Se}_{4-x}\text{Te}_x$ sample. The parent sample showed a rapid transition to a superconducting state at 3.5 K, with an initial R -value of 41, indicating a high degree of homogeneity in the undoped sample. The RRR values indicate that Te doping introduces disorder in the $\text{CuRh}_2\text{Se}_{4-x}\text{Te}_x$ system, suppressing the critical temperature T_c . In addition, the subsequent decrease in RRR also indicates an enhanced effect of electron scattering. In the temperature range of 300 K to 1.8 K, the resistivity of polycrystalline samples of $\text{CuRh}_2\text{Se}_{4-x}\text{Te}_x$ ($2.8 \leq x \leq 4.0$) was measured. However, no superconducting transition was observed in the samples when the temperature was lowered to 1.8 K, as shown in **Fig. 3(c)**. The ZFC measurements under 30 Oe magnetic field were applied to detect the diamagnetism of superconducting $\text{CuRh}_2\text{Se}_{4-x}\text{Te}_x$ ($0 \leq x$

≤ 0.28) samples in the temperature range of 1.8 - 4.5 K as depicted in **Fig. 3(d)**. The decreasing trend of spinel $\text{CuRh}_2\text{Se}_{4-x}\text{Te}_x$ ($0 \leq x \leq 0.28$) compound. As a result, T_c decreases almost to 3.05 K at $x = 0.1$. Significantly, T_c also reduces with increasing doping content of Te. The trend of T_c shows great agreement with the R-T results at slightly lower levels due to the suppression of the applied magnetic field. However, the T_c is not as steep as expected. We suggest that this phenomenon originates from the decay of the Meissner screen current, which is common in polycrystalline samples. Next, we systematically studied the spinel $\text{CuRh}_2\text{Se}_{4-x}\text{Te}_x$ ($0 \leq x \leq 0.28$). We also performed upper and lower critical magnetic field fitting tests on polycrystalline samples.

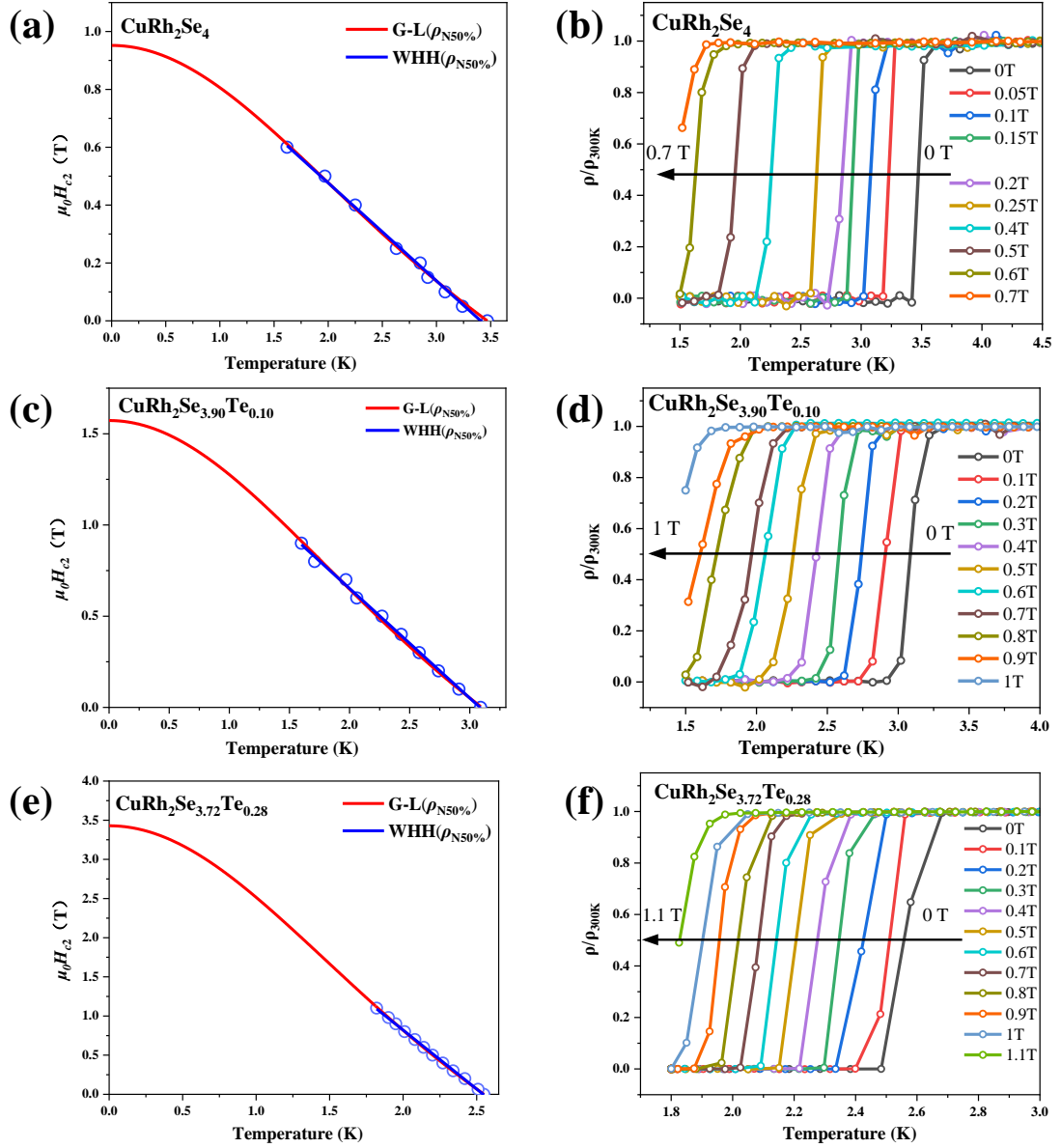


Fig. 4. The temperature dependence measurement of the upper critical $\mu_0 H_{c2}(0)$ fields for $\text{CuRh}_2\text{Se}_{4-x}\text{Te}_x$ ($x = 0, 0.1, 0.28$); (a), (c), and (e) show the refinements of $\text{CuRh}_2\text{Se}_{4-x}\text{Te}_x$ ($x = 0, 0.1, 0.28$), respectively. The red curve exhibits the refinement by G-L theory, while the blue curve displays the refinement by the WHH model; (b), (d), and (f) show the detailed process for determining $\mu_0 H_{c2}(0)$.

The upper critical field $\mu_0 H_{c2}(0)$ was systematically investigated by R-T measurements. The measurement procedure for $\text{CuRh}_2\text{Se}_{4-x}\text{Te}_x$ ($x = 0, 0.1, 0.28$) is shown in **Fig. 4(a)-4(f)**. The distribution of points exhibits good function compliance, as demonstrated in **Fig. 4(a), 4(c), and 4(e)**. Werthamer-Helfand-Hohenburg (WHH) and Ginzberg-Landau (G-L) theories of $\mu_0 H_{c2}(0)$ theory are based on data plots for the $\mu_0 H_{c2}(0)$, which are established using the 50% criterion of the normal state resistivity value. From **Fig. 4(b), 4(d), and 4(f)**, it can be seen that T_c exhibits a significant shift toward the low-temperature region as the applied magnetic field strength increases. The $d\mu_0 H_{c2}(0)/dT$ is the slope of the plot around T_c used in the simplified WHH equation: $\mu_0 H_{c2}(0) = -0.693 T_c \left(\frac{d\mu_0 H_{c2}}{dT} \right) |_{T=T_c}$. As dirty limits for the WHH model, the calculated values for CuRh_2Se_4 , $\text{CuRh}_2\text{Se}_{3.9}\text{Te}_{0.1}$, and $\text{CuRh}_2\text{Se}_{3.72}\text{Te}_{0.28}$ are 0.89(2) T, 1.29(3) T, and 2.60(2) T, respectively. Due to the Bowling Limit effect, the $\mu_0 H_{c2}(0)$ calculated by the WHH model has to be smaller than the Pauling limit field $\mu_0 H^{\text{Pauli}} = 1.86 T_c$ [36]. In this case, the $\mu_0 H^{\text{Pauli}}$ is 6.32(2) T, 5.76(2) T, and 4.65(3) T for CuRh_2Se_4 , $\text{CuRh}_2\text{Se}_{3.9}\text{Te}_{0.1}$, and $\text{CuRh}_2\text{Se}_{3.72}\text{Te}_{0.28}$, respectively. The $\mu_0 H_{c2}(0)$ also follows a functional distribution based on G-L theory: $\mu_0 H_{c2}(T) = \mu_0 H_{c2}(0) \times \frac{(1-(T/T_c)^2)}{(1+(T/T_c)^2)}$, where $\mu_0 H_{c2}(0)$ can be calculated. The estimated values of $\mu_0 H_{c2}(0)$ for CuRh_2Se_4 , $\text{CuRh}_2\text{Se}_{3.9}\text{Te}_{0.1}$, and $\text{CuRh}_2\text{Se}_{3.72}\text{Te}_{0.28}$ are 0.95(2) T, 1.57(4) T, and 3.44(1) T, respectively. The results indicate that replacing Se with Te can greatly raise the $\mu_0 H_{c2}(0)$, even though there is a minor difference between the values of $\mu_0 H_{c2}(0)$ derived using WHH modeling and G-L theory. We think that Te substitution effects are the source of the rise in the $\mu_0 H_{c2}(0)$. The RRR depicted in **Fig.**

S4 serves as a measure of disorder, where a diminishing value signifies heightened disorder. Upon doping the Te element into the pristine CuRh_2Se_4 spinel, a stark decrease in the RRR value is evident, illustrating the effective role of Te as a scattering center. Thus, the inclusion of Te elements notably exacerbates the disorder. This leads to intensified electron scattering and a reduction in the mean free path of carriers [37-40]. Based on these factors, we hypothesize that the shorter coherence length resulting from impurity scattering may be the reason for the augmentation of $\mu_0 H_{c2}(0)$ in Te-doped samples. Then, we measured the M-H curves at various temperatures to find the lower critical transition magnetic field $\mu_0 H_{c1}(0)$. The parent sample CuRh_2Se_4 with the greatest T_c was chosen for testing. The details of the $\mu_0 H_{c1}(0)$ test is displayed in **Fig. S5**. All values with corresponding temperatures are shown in **Fig. S5(a)** and correspond to the equation $\mu_0 H_{c1}^*(T) = \mu_0 H_{c1}^*(0) (1 - (T/T_c)^2)$, which is indicated by the red solid line. The calculated $\mu_0 H_{c1}(0)$ is 143(6) Oe, which is close to the value previously reported in the literature (100 Oe) [29]. In addition, the lower critical field is calculated by the equation $\mu_0 H_{c1}(0) = \mu_0 H_{c1}^*(0)/(1-N)$ when considering an N value of 0.5. Thus, the modified lower critical field $\mu_0 H_{c1}(0)$ is 286 Oe. The inset of **Fig. S5(a)** shows the field-dependent magnetization intensity measurements of the spinel CuRh_2Se_4 superconductor at different temperatures below T_c . The magnetization intensity M and the external magnetic field H show a linear association in the range of low external magnetic field strengths, as indicated by the equation $M_{\text{fit}} = e + fH$. In this case, f stands for the linear relationship's slope, and e for the intercept [40]. **Fig. S5(b)** shows the M -

M_{fit} curve. The field where the magnetization intensity starts to deviate from the linear response is the uncorrected lower critical field $\mu_0 H_{c1}^*(0)$ for that temperature.

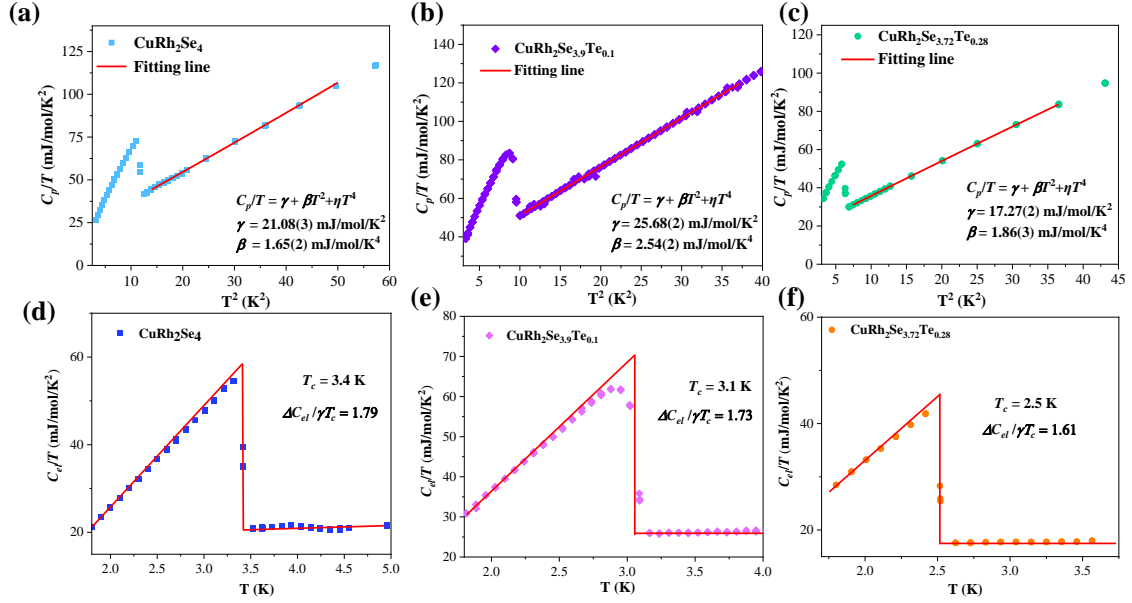


Fig. 5 The temperature-dependent specific heat for the spinel $\text{CuRh}_2\text{Se}_{4-x}\text{Te}_x$ ($x = 0, 0.1, 0.28$).

(a), (b), and (c) The C_p/T vs T^2 curves, fitted with the equation $C_p/T = \gamma + \beta T^2 + \eta T^4$. (d), (e), and (f) Electronic contribution to the heat capacity divided by temperature (C_{el}/T) vs temperature T without an applied magnetic field.

After observing the zero resistivity and the Meissner effect during magnetization, we further performed specific heat measurements of $\text{CuRh}_2\text{Se}_{4-x}\text{Te}_x$ ($x = 0, 0.1, 0.28$), as shown in **Fig. 5**. The heat capacity data above T_c can be fitted by the equation $C_p/T = \gamma + \beta T^2 + \eta T^4$, where two-term $\beta T^2 + \eta T^4$ are used to express the phonon contribution, and γ represents the normal state electronic specific heat coefficient. The values of γ and β for the CuRh_2Se_4 are $21.08(3) \text{ mJ mol}^{-1} \text{ K}^{-2}$ and $1.65(2) \text{ mJ mol}^{-1} \text{ K}^{-4}$, respectively. In addition, the values of γ and β for the $\text{CuRh}_2\text{Se}_{3.72}\text{Te}_{0.28}$ are $17.27(2) \text{ mJ mol}^{-1} \text{ K}^{-2}$ and

1.86(3) mJ mol⁻¹ K⁻⁴, respectively. The **Figs. 5(d), (e), and (f)** display the C_{el}/T vs T curves. The estimated T_c obtained from the equal-entropy construction agrees with the resistivity and magnetization measurements of the polycrystalline sample. The normalized specific heat jump value $\Delta C_{el}/\gamma T_c$ is 1.79 for CuRh₂Se₄ and 1.61 for CuRh₂Se_{3.72}Te_{0.28}, which is slightly above the Bardeen - Cooper - Schrieffer (BCS) weak coupling limit value of 1.43, indicating the presence of bulk superconductivity. The Debye temperature (Θ_D) is calculated as $\Theta_D = (12\pi^4 n R / 5\beta)^{1/3}$, where n is the number of atoms in the unit of the formula, and R is the molar gas constant. The calculated Θ_D is 202 K for CuRh₂Se₄ and 194 K for CuRh₂Se_{3.72}Te_{0.28}. Given the Θ_D and T_c , the electron-phonon coupling constant λ_{ep} of CuRh₂Se₄ and CuRh₂Se_{3.72}Te_{0.28} can be calculated to be 0.64 and 0.59 with $\mu^* = 0.13$ using McMillan's equation:

$$\lambda_{ep} = \frac{1.04 + \mu^* \ln\left(\frac{\Theta_D}{1.45T_c}\right)}{\left(1 - 1.62\mu^*\right) \ln\left(\frac{\Theta_D}{1.45T_c}\right) - 1.04}, \text{ respectively. [41].}$$

located at the Fermi energy level $N(E_F)$ can also be estimated using the formula

$$N(E_F) = \frac{3}{\pi^2 k_B^2 (1 + \lambda_{ep})} \gamma \text{ with values } \gamma \text{ and } \lambda_{ep}.$$

Since the parent sample CuRh₂Se₄ is close to CuRh₂Se_{3.9}Te_{0.1} in terms of T_c and $N(E_F)$, we chose to compare the parent sample CuRh₂Se₄ with the highest doped sample CuRh₂Se_{3.72}Te_{0.28}. The $N(E_F)$ of 5.5 states/eV f.u. for the parent CuRh₂Se₄ is significantly higher than that of 4.6 states/eV f.u. for the highest doped CuRh₂Se_{3.72}Te_{0.28}. This suggests that the doping of the Te element may change the electronic band structure of the material, including tuning the parameters of the DOSs near the Fermi energy level and electronic bandwidth. Such changes may affect the superconducting pairing mechanism and hence the T_c . In addition, **Table 1** summarizes the parameters of the superconducting properties of CuRh₂Se_{4-x}Te_x ($x=0, 0.1, 0.28$) and the spinel compounds CuRh₂S₄, CuRh₂Se₄ and CuRh_{1.88}Pt_{0.12}Se₄ doped samples from other papers. Furthermore, the Te elemental doping in the polycrystalline

samples of $\text{CuRh}_2(\text{S}_{1-x}\text{Te}_x)_4$ ($0 \leq x \leq 0.1$) leads to a decrease in the T_c . Once Te is introduced, the lattice constant a increases. There is a strong correlation between the T_c and the lattice constant a . The suppression of T_c is most likely due to the substitution of Te, which reduces the density of states at the $N(E_F)$ [42]. Besides, transport and magnetization strength measurements show that the T_c of FeSe single crystals decreases with increasing Te doping. The overdoping of Te produces more non-superconducting regions, which rapidly reduces the flux pinning energy and critical current density [43]. Taken together, Te element doping may affect the electronic structure and interactions of the material and break the stability of the superconducting pairing, which leads to a decrease in the T_c .

Table 1 summarizes the superconducting property parameters of spinel compounds CuRh_2S_4 , CuRh_2Se_4 , and CuRh_2Se_4 doped samples. The comparison of superconducting characteristic parameters for spinel compounds.

Compound	CuRh_2S_4	$\text{CuRh}_{1.88}\text{Pt}_{0.12}\text{Se}_4$	CuRh_2Se_4	$\text{CuRh}_2\text{Se}_{3.9}\text{Te}_{0.1}$	$\text{CuRh}_2\text{Se}_{2.72}\text{Te}_{0.28}$	CuRh_2Se_4
	[13]	[29]	[this work]	[this work]	[this work]	[29]
T_c (K)	3.5	3.84(2)	3.4	3.11	2.5	3.38(1)
$\mu_0 H_{c1}(0)$ (Oe)	-	168(12)	-	143(6)	-	220(6)
$\mu_0 H_{c2}(0)$ (T)						
$(\rho^{50\%_N G-L}$ theory)	-	4.93(1)	0.95(2)	1.57(4)	3.44(1)	1.00(1)
$\mu_0 H^{\text{Pauli}}$	-	7.176(4)	6.32(2)	5.76(2)	4.65(3)	6.311(2)
$-d\mu_0 H_{c2}(0)/dT_c$ (T/K)	0.614	1.418	0.347(3)	0.601(5)	1.503(2)	0.352(8)
γ (mJ mol ⁻¹ K ⁻²)	26.9	-	21.08(3)	25.68(2)	17.27(2)	21.4
β (mJ mol ⁻¹ K ⁻⁴)	-	-	1.65(2)	2.54(2)	1.86(3)	-
$\Delta C_{el}/\gamma T_c$	1.89	-	1.79	1.73	1.61	1.68

Θ_D (K)	258	-	202	175	194	218
λ_{ep}	0.66	-	0.64	0.65	0.59	0.63
$N(E_F)$ (states/eV f.u.)	-	-	5.5	6.6	4.6	-

The electronic phase diagrams of the spinel superconductor $\text{CuRh}_2\text{Se}_{4-x}\text{Te}_x$ ($0 \leq x \leq 0.28$) and high doping levels of layered compound $\text{CuRh}_2\text{Se}_{4-x}\text{Te}_x$ ($2.8 \leq x \leq 4.0$) are summarized in **Fig. 6**. The T_c obtained from the R-T experimental results is summarized as a curve related to the Te doping concentration. As can be seen, T_c shows a decreasing trend with increasing Te substitution, yet the $\mu_0 H_{c2}(0)$ enhances with the Te doping content in the spinel $\text{CuRh}_2\text{Se}_{4-x}\text{Te}_x$ ($0 \leq x \leq 0.28$) compositions. However, no superconductivity is found for the layered compound $\text{CuRh}_2\text{Se}_{4-x}\text{Te}_x$ ($2.8 \leq x \leq 4.0$) from 300 K to 1.8 K.

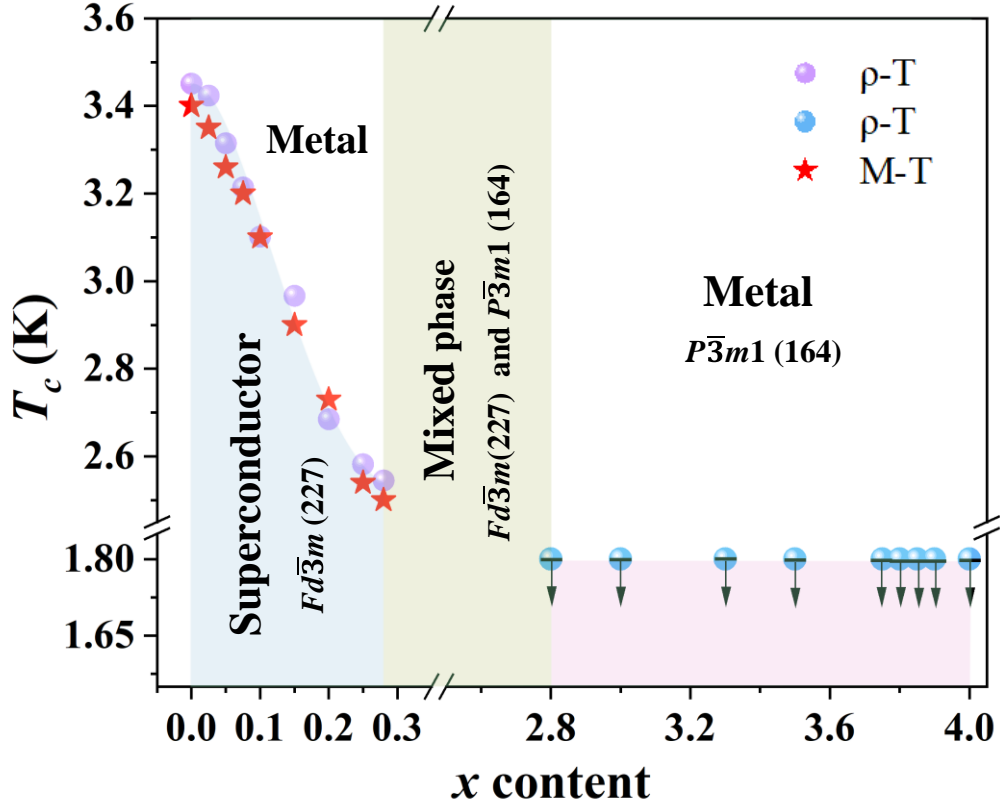


Fig. 6 The electronic phase diagram for the spinel superconductor $\text{CuRh}_2\text{Se}_{4-x}\text{Te}_x$ ($0 \leq x \leq 0.28$) and the layered compound $\text{CuRh}_2\text{Se}_{4-x}\text{Te}_x$ ($2.8 \leq x \leq 4.0$) vs Te content.

CONCLUSIONS

We have conducted a systematic study of the effect of Te doping on the spinel CuRh_2Se_4 . XRD analysis revealed that the low-doping $\text{CuRh}_2\text{Se}_{4-x}\text{Te}_x$ ($0 \leq x \leq 0.28$) compositions crystallized in the spinel structure with the space group $Fd\bar{3}m$ (227), while the high-doping $\text{CuRh}_2\text{Se}_{4-x}\text{Te}_x$ ($2.8 \leq x \leq 4.0$) compounds crystallized in the layered structure with the space group $P\bar{3}m1$ (164). The XRD refinement data show that the lattice parameters increase with increasing Te doping. Resistivity and magnetization measurements show that T_c decreases almost linearly with increasing Te content in the spinel $\text{CuRh}_2\text{Se}_{4-x}\text{Te}_x$ ($0 \leq x \leq 0.28$) system, whereas the highly doped

levels of layered compound $\text{CuRh}_2\text{Se}_{4-x}\text{Te}_x$ ($2.8 \leq x \leq 4.0$) did not exhibit superconducting properties. The RRR values indicate that Te doping introduces disorder in the $\text{CuRh}_2\text{Se}_{4-x}\text{Te}_x$ system. Notably, the highest-doped $\text{CuRh}_2\text{Se}_{3.72}\text{Te}_{0.28}$ spinel has an enhanced upper critical magnetic field $\mu_0 H_{c2}(0)^{GL} = 3.44(1)$ T. Besides, the zero-field heat capacity indicates the presence of bulk superconductivity and the variation of the density of states is obtained. Our results reveal that Te doping can significantly modulate the superconductivity and structure of the spinel CuRh_2Se_4 . Te elemental doping affects the electronic structure and interactions of the material and destabilizes the superconducting pairs, leading to a decrease in T_c . These findings can give new insight for further discovery of other new spinel superconductors or enhance the superconductivity of the original spinels.

Notes

The authors declare no competing financial interest

ACKNOWLEDGMENT

This work is supported by the National Natural Science Foundation of China (12274471, 11922415), Guangdong Basic and Applied Basic Research Foundation (2022A1515011168), 2024 Basic and Applied Basic Research Topic (Science and Technology Elite "Navigation" Project“, 2024A04J6415). The experiments reported were conducted at the Guangdong Provincial Key Laboratory of Magnetoelectric Physics and Devices, No. 2022B1212010008.

REFERENCES

- [1] J. Hemberger, H.A.K. von Nidda, V. Tsurkan, A. Loidl, Large Magnetostriction and Negative Thermal Expansion in the Frustrated Antiferromagnet ZnCr_2Se_4 , *Physical Review Letters* 98(14) (2007) 147203.

- [2] A.P. Ramirez, R.J. Cava, J. Krajewski, Colossal magnetoresistance in Cr-based chalcogenide spinels, *Nature* 386(6621) (1997) 156-159.
- [3] Z. Yang, S. Tan, Z. Chen, Y. Zhang, Magnetic polaron conductivity in FeCr_2S_4 with the colossal magnetoresistance effect, *Physical Review B* 62(21) (2000) 13872-13875.
- [4] S. Weber, P. Lunkenheimer, R. Fichtl, J. Hemberger, V. Tsurkan, A. Loidl, Colossal Magnetocapacitance and Colossal Magnetoresistance in HgCr_2S_4 , *Physical Review Letters* 96(15) (2006) 157202.
- [5] K. Ohgushi, T. Ogasawara, Y. Okimoto, S. Miyasaka, Y. Tokura, Gigantic Kerr rotation induced by a $d-d$ transition resonance in $M\text{Cr}_2\text{S}_4$ ($M = \text{Mn, Fe}$), *Physical Review B* 72(15) (2005) 155114.
- [6] J. Hemberger, P. Lunkenheimer, R. Fichtl, H.A. Krug von Nidda, V. Tsurkan, A. Loidl, Relaxor ferroelectricity and colossal magnetocapacitive coupling in ferromagnetic CdCr_2S_4 , *Nature* 434(7031) (2005) 364-367.
- [7] N. H. Van Maaren, G.M. Schaeffer, F.K. Lotgering, Superconductivity in sulpho- and selenospinel, *Phys. Lett. A* 25(3) (1967) 238-239.
- [8] M. Robbins, R.H. Willens, R.C. Miller, Superconductivity in the spinels CuRh_2S_4 and CuRh_2Se_4 , *Solid State Communications* 5(12) (1967) 933-934.
- [9] D.C. Johnston, H. Prakash, W.H. Zachariasen, R. Viswanathan, High temperature superconductivity in the Li Ti O ternary system, *Mater. Res. Bull.* 8(7) (1973) 777-784.
- [10] W. Hu, Z. Feng, B.-C. Gong, G. He, D. Li, M. Qin, Y. Shi, Q. Li, Q. Zhang, J. Yuan, B. Zhu, K. Liu, T. Xiang, L. Gu, F. Zhou, X. Dong, Z. Zhao, K. Jin, Emergent superconductivity in single-crystalline MgTi_2O_4 films via structural engineering, *Physical Review B* 101(22) (2020) 220510.
- [11] T. Bitoh, T. Hagino, Y. Seki, S. Chikazawa, S. Nagata, Superconductivity in Thiospinel CuRh_2S_4 , *Journal of the Physical Society of Japan* 61(8) (1992) 3011-3012.
- [12] M. Ito, J. Hori, H. Kurisaki, H. Okada, A.J.P. Kuroki, N. Ogita, M. Udagawa, H. Fujii, F. Nakamura, T. Fujita, T. Suzuki, Pressure-Induced Superconductor-Insulator Transition in the Spinel Compound CuRh_2S_4 , *Physical Review Letters* 91(7) (2003)
- [13] T. Shirane, T. Hagino, Y. Seki, T. Bitoh, S. Chikazawa, S. Nagata, Superconductivity in Selenospinel CuRh_2Se_4 , *Journal of the Physical Society of Japan* 62(1) (1993) 374-375.
- [14] R.N. Shelton, D.C. Johnston, H. Adrian, Measurement of the pressure dependence of T_c for superconducting spinel compounds, *Solid State Communications* 20(11) (1976) 1077-1080.
- [15] T. Hagino, Y. Seki, N. Wada, S. Tsuji, T. Shirane, K.-i. Kumagai, S. Nagata, Superconductivity in spinel-type compounds CuRh_2S_4 and CuRh_2Se_4 , *Physical Review B* 51(18) (1995) 12673-12684.
- [16] H. Suzuki, T. Furubayashi, G. Cao, H. Kitazawa, A. Kamimura, K. Hirata, T. Matsumoto, Metal-Insulator Transition and Superconductivity in Spinel-Type System $\text{Cu}_{1-x}\text{Zn}_x\text{Ir}_2\text{S}_4$, *Journal of the Physical Society of Japan* 68(8) (1999) 2495-2497.
- [17] G. Cao, H. Kitazawa, H. Suzuki, T. Furubayashi, K. Hirata, T. Matsumoto, Superconductivity in Zn-doped CuIr_2S_4 , *Physica C: Superconductivity* 341-348 (2000) 735-736.

- [18] H. Luo, T. Klimczuk, L. Muehler, L. Schoop, D. Hirai, M.K. Fuccillo, C. Felser, R.J. Cava, Superconductivity in the $\text{Cu}(\text{Ir}_{1-x}\text{Pt}_x)_2\text{Se}_4$ spinel, *Physical Review B* 87(21) (2013) 214510.
- [19] Y.-Y. Jin, S.-H. Sun, Y.-W. Cui, Q.-Q. Zhu, L.-W. Ji, Z. Ren, G.-H. Cao, Bulk superconductivity and Pauli paramagnetism in nearly stoichiometric CuCo_2S_4 , *Physical Review Materials* 5(7) (2021) 074804.
- [20] T. Oda, M. Shirai, N. Suzuki, K. Motizuki, Electronic band structure of sulphide spinels CuM_2S_4 (M=Co, Rh,Ir), *Journal of Physics: Condensed Matter* 7(23) (1995) 4433.
- [21] R.M. Fleming, F.J. DiSalvo, R.J. Cava, J.V. Waszczak, Observation of charge-density waves in the cubic spinel structure CuV_2S_4 , *Physical Review B* 24(5) (1981) 2850-2853.
- [22] N. Le Nagard, A. Katty, G. Collin, O. Gorochov, A. Willig, Elaboration, structure cristalline et proprietes physiques (transport, susceptibilite magnetique et R.M.N.) du spinelle CuV_2S_4 , *Journal of Solid State Chemistry* 27(3) (1979) 267-277.
- [23] T. Hagino, Y. Seki, S. Nagata, Metal - insulator transition in CuIr_2S_4 : Comparison with CuIr_2Se_4 , *Physica C: Superconductivity* 235-240 (1994) 1303-1304.
- [24] T. Furubayashi, T. Kosaka, J. Tang, T. Matsumoto, Y. Kato, S. Nagata, Pressure Induced Metal-Insulator Transition of Selenospinel CuIr_2Se_4 , *Journal of the Physical Society of Japan* 66(5) (1997) 1563-1564.
- [25] T. Furubayashi, T. Matsumoto, T. Hagino, S. Nagata, Structural and Magnetic Studies of Metal-Insulator Transition in Thiospinel CuIr_2S_4 , *Journal of the Physical Society of Japan* 63(9) (1994) 3333-3339.
- [26] T. Hagino, T. Tojo, T. Atake, S. Nagata, Metal-insulator transition at 230 K in a new thiospinel CuIr_2S_4 , *Philosophical Magazine B* 71(5) (1995) 881-894.
- [27] G. Oomi, T. Kagayama, I. Yoshida, T. Hagino, S. Nagata, Effect of pressure on the metal-insulator transition temperature in thiospinel CuIr_2S_4 , *Journal of Magnetism and Magnetic Materials* 140-144 (1995) 157-158.
- [28] G. Cao, T. Furubayashi, H. Suzuki, H. Kitazawa, T. Matsumoto, Y. Uwatoko, Suppression of metal-to-insulator transition and appearance of superconductivity in $\text{Cu}_{1-x}\text{Zn}_x\text{Ir}_2\text{S}_4$, *Physical Review B* 64(21) (2001) 214514.
- [29] Y. He, Y.-X. You, L. Zeng, S. Guo, H. Zhou, K. Li, Y. Huang, P. Yu, C. Zhang, C. Cao, H. Luo, Superconductivity with the enhanced upper critical field in the Pt-doped CuRh_2Se_4 spinel, *Physical Review B* 105(5) (2022) 054513.
- [30] R. Mao, Z. Wu, Z. Wang, Z. Pan, M. Xu, Z. Wang, Effect of Te-doping on the superconducting characteristics of FeSe single crystal, *Journal of Alloys and Compounds* 809 (2019) 151851.
- [31] Y. Zhang, T. Wang, Z. Wang, Z. Xing, Effects of Te- and Fe-doping on the superconducting properties in $\text{Fe}_y\text{Se}_{1-x}\text{Te}_x$ thin films, *Scientific Reports* 12(1) (2022) 391.
- [32] K. W. Yeh, H. C. Hsu, T. W. Huang, P. M. Wu, Y. L. Huang, T. K. Chen, J. Y. Luo, M. K. Wu, Se and Te Doping Study of the FeSe Superconductors, *Journal of the Physical Society of Japan* 77(Suppl.C) (2008) 19-22.

- [33] D. Yan, S. Wang, Y. S. Lin, G. H. Wang, Y. J. Zeng, M. Boubeche, Y. He, J. Ma, Y. H. Wang, D. X. Yao, H. X. Luo, NbSeTe—a new layered transition metal dichalcogenide superconductor, *J. Phys.: Condens. Matter* 32 (2020) 025702.
- [34] H.-T. Wang, L.-J. Li, D.-S. Ye, X.-H. Cheng, Z.-A. Xu, Effect of Te doping on superconductivity and charge-density wave in dichalcogenides 2H-NbSe_{2-x}Te_x ($x = 0, 0.1, 0.2$), *Chinese Physics* 16(8) (2007) 2471.
- [35] J.D. Splett, D.F. Vecchia, L.F. Goodrich, A comparison of methods for computing the residual resistivity ratio of high-purity niobium, *Journal of research of the National Institute of Standards and Technology* 116(1) (2011) 489.
- [36] A.M. Clogston, Upper Limit for the Critical Field in Hard Superconductors, *Physical Review Letters* 9(6) (1962) 266-267.
- [37] X.-L. Wang, S.X. Dou, M.S.A. Hossain, Z.X. Cheng, X.Z. Liao, S.R. Ghorbani, Q.W. Yao, J.H. Kim, T. Silver, Enhancement of the in-field J_c of MgB₂ via SiCl₄ doping, *Physical Review B* 81(22) (2010) 224514.
- [38] K.S.B. De Silva, X. Xu, X.L. Wang, D. Wexler, D. Attard, F. Xiang, S.X. Dou, A significant improvement in the superconducting properties of MgB₂ by co-doping with graphene and nano-SiC, *Scripta Materialia* 67(10) (2012) 802-805.
- [40] H. Luo, W. Xie, J. Tao, I. Pletikovic, T. Valla, G.S. Sahasrabudhe, G. Osterhoudt, E. Sutton, K.S. Burch, E.M. Seibel, J.W. Krizan, Y. Zhu, R.J. Cava, Differences in Chemical Doping Matter: Superconductivity in Ti_{1-x}Ta_xSe₂ but Not in Ti_{1-x}Nb_xSe₂, *Chemistry of Materials* 28(6) (2016) 1927-1935.
- [41] W.L. McMillan, Transition Temperature of Strong-Coupled Superconductors, *Physical Review* 167(2) (1968) 331-344.
- [42] N. Kijima, H. Yashiro, S. Nagata, Superconductivity in CuRh₂(S_{1-x}Te_x)₄ ($0 \leq x \leq 0.1$), *Journal of Physics and Chemistry of Solids* 57(11) (1996) 1635-1639.
- [43] R. Mao, Z. Wu, Z. Wang, Z. Pan, M. Xu, Z. Wang, Effect of Te-doping on the superconducting characteristics of FeSe single crystal, *Journal of Alloys and Compounds* 809 (2019) 151851.